Capillary Flow in a Noncircular Tube

Raffi M. Turian and Frederick D. Kessler
Dept. of Chemical Engineering, University of Illinois at Chicago, Chicago, IL 60607

The 1-D axial, laminar, Newtonian flow through a tube of uniform, but noncircular, cross-section is analyzed. The tube boundary is $r = R[1 + \epsilon f(\theta)]$, in which R is a reference radius, ϵ is a small parameter, and the function $f(\theta)$ of the polar angle is general, albeit subject to minimal constraints ensuring single-valuedness and quadrant symmetry. All results are determined as asymptotic expansions complete to terms $O(\epsilon^2)$, which include the velocity distribution, average velocity, volume flow rate, ratio of flow rates in the noncircular to that in a circular pipe of the same cross-sectional area, the friction factor-Reynolds number dependence, the permeability of packed beds comprising noncircular capillaries, kinetic-energy and momentum-flux correction factors, the capillary penetration rate under the influence of the capillary pressure and the equilibrium value of the capillary rise. Expressions are derived in terms of the general boundary function $f(\theta)$ and, for special cases, when $f(\theta) = \sin^{2k}\theta$ ($k = 1, 2, 3$) and $f(\theta) = \sin^2 k\theta$ with k a positive integer. The results provide quantitative measures of the effect of tube shape on flow properties and on imbibition and drainage from noncircular capillaries.

Introduction

The results presented are of a detailed analysis of the one-dimensional (1-D) axial flow of Newtonian fluids through a tube having a uniform cross-section and a noncircular boundary defined by $r = R[1 + \epsilon f(\theta)]$. The boundary is varied in shape through the choice of the function of the polar angle $f(\theta)$, and in degree through the magnitude of the small parameter ϵ, which may be positive or negative. While the hydrodynamic problem addressed in this article is intrinsically interesting in itself, our primary motivation is to develop a body of analytical solutions pertaining to well-defined flows, which can be used to probe various factors (in this case, flow geometry) affecting flow through packed beds and penetration of liquids into, or their removal from, granular media.

The analytical results developed are in the form of asymptotic expansions in the parameter ϵ, and include the velocity distribution, the average velocity, the volumetric flow rate, the ratio of volumetric flow rates in the tube to that in a circular tube of the same cross-section, the friction factor-Reynolds number dependence, the permeability of packed beds comprised of the noncircular capillaries, the equilibrium height, and the rate of penetration of liquid under the influence of capillary pressure in the tube.

Correspondence concerning this article should be addressed to R. M. Turian.

All results are derived complete to $O(\epsilon^2)$ for both the general form of the boundary function $f(\theta)$, as well as for the special choices $f(\theta) = \sin^{2k}\theta$ with $k = 1$, 2, or 3, and $f(\theta) = \sin^2 k\theta$ with k a positive integer. Carrying out the calculations completely to $O(\epsilon^2)$ is essential, because important boundary-shape effects turn out to be second-order effects. Increasing the value of the exponent k enhances the distortion of the boundary from the circular shape, while increasing the absolute value of ϵ increases the degree of the distortion. The results in terms of the general function $f(\theta)$ can be used to test other admissible boundary functions, which like the choice $f(\theta) = \sin^{2k}\theta$ or $\sin^2 k\theta$ need only be periodic to insure single-valuedness, and positive in the range 0 to 2π to insure quadrant symmetry. Poiseuille flow through noncircular tubes has been studied for various tube boundary shapes as described below.

This work differs in that the boundary can be varied in shape and degree through choice of the function $f(\theta)$ and the magnitude of ϵ. Furthermore, the results are in analytical form, and are complete to the order presented as all coefficients are whole fractions. This provides a more direct instrument for probing flow geometry effects. The hydrodynamic solution presented in this article can also be used to probe tube boundary shape effects on the heating of fluids. This associated convective heat-transfer analysis is deferred.

Previous Work

Steady 1-D velocity fields

The steady, fully-developed, incompressible, laminar flow of Newtonian fluids through noncircular conduits of uniform cross-section is governed by an equation in which the Laplacian in two dimensions of the velocity component $v_z(x, y)$, or in polar coordinates $v_z(r, \theta)$, is equal to a constant proportional to the axial pressure gradient (see Eq. 1). This is true, of course, provided that conditions are such that secondary flows are absent, which requires the Reynolds number to be circumscribed. Aside from the differential equation, the no slip condition must be satisfied on the conduit boundaries. The mathematical problem arises in many areas, including heat conduction and elasticity (torsion), and is extensively treated in the literature on mathematical physics.

Exact or approximate solutions have been obtained for axial 1-D flows through tubes of uniform cross-section having a variety of different boundary shapes; the method of solution depends on the tube shape. In what might be referred to as the semi-inverse method, the fact that many polynomials have constant Laplacians, combined with the finding that additionally in some cases equating the polynomial to zero yields the equation of a closed contour, are exploited to establish a solution. Under the circumstances, the product of the polynomial with the appropriate constant, chosen to satisfy the differential equation, will also vanish on the contour. Simple polynomial expressions for the axial velocity distribution for flow through pipes with elliptical and with equilateral triangular boundaries have been obtained using the semi-inverse method (Langlois, 1964). By contrast, the rectangular pipe, with sides $x = \pm a$, $y = \pm b$, has the polynomial $[(x^2 - a^2)(y^2 - a^2)] = 0$ as the equation of its boundary, but its Laplacian is not constant. Therefore, the solution for the rectangular pipe is derived as an infinite series using separation of variables (Dryden et al., 1956). These are examples of simply connected boundaries. The eccentric annular geometry is not a simply connected boundary. However, the bilinear transformation permits one to map the region between the pair of eccentric circles in the *x-y* plane onto a concentric ring in the transformed plane (Langlois, 1964). A detailed analysis of the axial flow through an eccentric annulus is given by Snyder and Goldstein (1965).

Studies pertaining to 1-D axial flows through a wide array of different tube geometries have been reported in the literature. They include analytical or numerical solutions, as well as experimental works. A comprehensive and detailed review of the literature on such flows has been presented by Shah and London (1978). Aside from the ones mentioned above, the flow geometries considered include isosceles, right-angled as well as general triangles, and sine, trapezoidal, rhombic, quadrilateral, polygonal, circular-sector, annular-sector, crescent-shaped, corrugated-wall, and cusped ducts.

Capillary flow through ducts

In the flows discussed above, the driving force consists of the pressure gradient, which is taken as a constant. In capillary flows, the driving force must include the effect of the capillary pressure, requiring knowledge of the meniscus shape. Washburn (1921) derived the equation for the height of the liquid in a circular capillary as a function of time by incorporating the capillary pressure in Poiseuille's expression for the average velocity, assuming the meniscus shape to be part of a sphere having the same radius as the capillary. Washburn's solution will be presented later in this article. The key to extending capillary flow analysis to other flow geometries is to determine what meniscus shape is appropriate and, perhaps to a lesser extent, what value of the contact angle is operative. Understanding capillary flow through noncircular conduits is fundamental to many operations: imbibition, separation, and/or displacement of liquids from porous materials, permeametry and mercury porosimetry.

A basic method for determining the shapes of menisci in noncircular geometries was proposed by Princen (1969a) using the capillary rise of a wetting liquid (or depression of a nonwetting liquid) between two parallel cylinders a small, though variable, distance apart. Provided that the equilibrium height of the column of liquid is much greater than the radius of the cylinders, the liquid surface is essentially vertical from the bulk surface to somewhat below the meniscus. Accordingly, one of the radii of curvature is infinite. The other, representing the radius of the circular arcs in the horizontal cross-section, is then determined, as a function of the distance between cylinders, through a geometrical construction in which a material balance, using the cross-sectional area and the equilibrium height of the liquid column corresponding to the assumed meniscus shape, provides the needed closure. Extensions of this idea to assemblies of more than two parallel equidistant cylinders and a cylinder and a plate, and to assemblies of horizontal parallel cylinders, have also been carried out by Princen (1969b, 1970). The method proposed by Princen was used by Mason et al. (1983) to determine meniscus curvature and capillary rise between two contacting rods and a plate, giving results which agreed well with experimental data. In a further, more extensive, application of the method, Mason and Morrow (1991) derived the meniscus curvature of perfectly wetting liquids for drainage/penetration in pores with a triangular cross-section of all possible shapes. A notable outcome of this work was the finding that the appropriate normalized shape factor for capillary action in triangular pores is the ratio of the cross-sectional area to the square of the perimeter. This is tantamount to using the hydraulic radius in place of $(R/2)$ in the capillary pressure term for circular tubes (Eqs. 45 and 51). The same finding has been confirmed by Kim and Whitesides (1997) in a careful experimental study of the dynamics of imbibition of liquid prepolymers into micrometer-scale rectangular capillaries.

Applications of capillary phenomena abound in industry and in nature. Princen's (1970) studies on equilibrium configurations of liquids within assemblies of parallel horizontal rods provide models for wetting of textiles, while Marmur's (1988) analysis of the kinetics of radial capillary flow between two flat plates is an idealization of liquid penetration into thin porous media such as ink into paper. The motivation for substantially most of the research on capillary flow, like that of the present work, is to establish a basis for understanding liquid flow within porous structures; mercury porosimetry, oil displacement, wetting or dewatering of granular materials, and migration through soil. Penetration through packings of spherical particles has been investigated by Mason and Morrow (1994) using a combination of a method proposed by Mayer and Stowe (1965), aimed at relating the breakthrough

pressure in mercury penetration to particle radius and packing arrangement, with Princen's procedure for deducing meniscus shape. The results suggest that the effect of the liquid contact angle is moderated by the compensating effect of the converging-diverging geometry. Further, experiments indicate that inherent packing-particle surface roughness has an effect on the operative value of the contact angle. The nature of the operative contact angle in mercury intrusion through clusters of particles has been examined by Huisman (1983), while Smith and Stermer (1986) have investigated the use of mercury porosimetry in the characterization of the structure of random packings of microspheres. The role of the contact angle in interpreting capillary flows is complicated when the flow geometry is complex and is, in any case, somewhat uncertain when the fluid is in motion; different values are operative depending upon whether the meniscus is receding, advancing or at equilibrium (Rillaerts and Joos, 1980; Bracke et al., 1989). The effects of surface roughness and contact angle hysteresis have been treated by Bracke et al. (1988). The result of modification of the contact angle on the dynamics of capillary flow, and on Washburn's relation, has been examined in a series of articles (Joos et al., 1990; Remoortere and Joos, 1991, 1993).

Poiseuille Flow through Noncircular Tube

We use cylindrical coordinates in dimensionless form, and consider the steady-state axial flow of a Newtonian fluid through a straight tube of a uniform cross-section having a circumference in the form of a slightly distorted circle with a radius given by $R[1+\epsilon f(\theta)]$, in which ϵ is a small parameter. The function of the polar angle $f(\theta)$ can be chosen to vary the shape of the boundary, though its prescription will be restricted by requirements of single-valuedness, and, also, if desired, by quadrant symmetry. Appropriate forms for this function will be considered below. The dimensionless axial velocity component $w(r,\theta)$ is governed by the equation

$$\frac{1}{r}\frac{\partial}{\partial r}\left(r\frac{\partial w}{\partial r}\right)+\frac{1}{r^2}\frac{\partial^2 w}{\partial \theta^2}+4=0 \tag{1}$$

subject to the boundary conditions

$$r=0: \qquad w_r=w_\theta=0 \tag{2}$$

$$r=1+\epsilon f(\theta) \qquad w=0 \tag{3}$$

The r and θ subscripts here denote partial derivatives. All variables in these equations are dimensionless; w is nondimensionalized with respect to the reference velocity $[R^2(-dp/dz)/4\mu]$, and r is nondimensionalized with respect to the reference radius R. We seek a solution of Eqs. 1–3 for $\epsilon \ll 1$.

The transformation $w(r,\theta)=[(1-r^2)-u(r,\theta)]$ in Eq. 1 yields the homogeneous equation

$$L^2u \equiv \frac{1}{r}\frac{\partial}{\partial r}\left(r\frac{\partial u}{\partial r}\right)+\frac{1}{r^2}\frac{\partial^2 u}{\partial \theta^2}=0 \tag{4}$$

$$r=0: \qquad u_r=u_\theta=0 \tag{5}$$

$$r=1+\epsilon f(\theta): \quad u=(1-r^2)=-2\epsilon f(\theta)-\epsilon^2 f^2(\theta) \tag{6}$$

For small ϵ, the solution of Eqs. 4–6 is in the form of the expansion

$$u(r,\theta) \quad u_0(r,\theta)+\epsilon u_1(r,\theta)+\epsilon^2 u_2(r,\theta)+\ldots. \tag{7}$$

The expression for u at the tube boundary, $r=1+\epsilon f(\theta)$, is then given by the expansion

$$\begin{aligned} u[1+\epsilon f(\theta),\theta] &\sim u_0[1+\epsilon f(\theta),\theta]+\epsilon u_1[1+\epsilon f(\theta),\theta] \\ &+\epsilon^2 u_2[1+\epsilon f(\theta),\theta]+\ldots \sim u_0(1,\theta)+\epsilon\{f(\theta)u_{0r}(1,\theta) \\ &+u_1(1,\theta)\}+\epsilon^2\{f^2(\theta)u_{0rr}(1,\theta) \\ &+f(\theta)u_{1r}(1,\theta)+u_2(1,\theta)\}+O(\epsilon^3) \end{aligned} \tag{8}$$

Using the second-order operator, L^2, defined in Eq. 4, the differential equation for u_0 is given by

$$L^2u_0=0; \quad \text{with } u_{0r}(0,\theta)=u_{0\theta}(0,\theta)=0, \quad \text{and} \quad u_0(1,\theta)=0 \tag{9}$$

It is clear from Eq. 9 that the solution is $u_0(r,\theta)=0$, and, using this result, the differential equations for u_1, and u_2 are

$$L^2u_1=0: \quad \text{with } u_{1r}(0,\theta)=u_{1\theta}(0,\theta)=0, \quad \text{and} \quad u_1(1,\theta)=-2f(\theta) \tag{10}$$

$$L^2u_2=0: \quad \text{with } u_{2r}(0,\theta)=u_{2\theta}(0,\theta)=0, \quad \text{and} \quad u_2(1,\theta)=-f^2(\theta)-f(\theta)u_{1r}(1,\theta) \tag{11}$$

As stated above r and θ subscripts in Eqs. 9 through 11 designate partial derivatives.

The solution of Eq. 10 for $u_1(r,\theta)$ is obtained using a separation of variables. The choice of the function $f(\theta)$ defining the boundary is still open. Without prescribing the specific form of $f(\theta)$ at this stage, we merely restrict its ultimate choice only to functions which are compatible with quadrant symmetry, resulting in a flow field comprised of four identical quadrants. Under these circumstances, the eigenvalues and eigenfunctions are determined by the requirements of symmetry, and, of course, single-valuedness. The resulting solution for $u_1(r,\theta)$ is given by

$$u_1(r,\theta)=\sum_{n=0}^{\infty} A_n r^{2n}\cos 2n\theta \tag{12}$$

in which the constants A_n are given by

$$A_0=-\frac{1}{\pi}\int_0^{2\pi} f(\theta)\,d\theta \tag{13}$$

$$A_n=-\frac{2}{\pi}\int_0^{2\pi} f(\theta)\cos 2n\theta\,d\theta \quad (n=1,2,3,\ldots) \tag{14}$$

Invoking the same symmetry requirements, and introducing the solution for u_1 into Eq. 11, we obtain the solution for

$u_2(r,\theta)$. This is given by

$$u_2(r,\theta) = \sum_{n=0}^{\infty} B_n r^{2n} \cos 2n\theta \tag{15}$$

in which the constants B_n $(n = 0, 1, 2, \ldots)$ are given by

$$B_0 = -\frac{1}{2\pi}\int_0^{2\pi} f^2(\theta)\, d\theta + \frac{2}{\pi^2}\sum_{m=1}^{\infty} m\left[\int_0^{2\pi} f(\theta)\cos 2m\theta\, d\theta\right]^2 \tag{16}$$

and

$$B_n = -\frac{1}{\pi}\int_0^{2\pi} f^2(\theta)\cos 2n\theta\, d\theta + \frac{4}{\pi^2}\sum_{m=1}^{\infty} m\int_0^{2\pi} f(\theta)\cos 2m\theta\cos 2n\theta\, d\theta \int_0^{2\pi} f(\theta)\cos 2m\theta\, d\theta \quad (n = 1, 2, 3, \ldots) \tag{17}$$

The volume rate of flow Q through the tube is given by the equation

$$Q \approx \frac{\pi R^4}{8\mu}\left(-\frac{dp}{dz}\right)\left\{\frac{2}{\pi}\int_0^{2\pi}\int_0^{1+\epsilon f(\theta)}\left[1 - r^2 - \epsilon\sum_{n=0}^{\infty} A_n r^{2n} \times \cos 2n\theta - \epsilon^2\sum_{n=0}^{\infty} B_n r^{2n}\cos 2n\theta + O(\epsilon^3)\right] r\, dr\, d\theta\right\}$$
$$\approx \frac{\pi R^4}{8\mu}\left(-\frac{dp}{dz}\right)\left(1 + \epsilon Q_1^* + \epsilon^2 Q_2^* + \ldots\right) \tag{18}$$

in which Q_1^* and Q_2^* are given by

$$Q_1^* = -2A_0 = \frac{2}{\pi}\int_0^{2\pi} f(\theta)\, d\theta \tag{19}$$

$$Q_2^* = -\frac{2}{\pi}\int_0^{2\pi} f^2(\theta)\, d\theta - \frac{2}{\pi}\sum_{n=0}^{\infty} A_n\int_0^{2\pi} f(\theta)\cos 2n\theta\, d\theta - 2B_0 \tag{20}$$

The cross-sectional area of the tube is given by

$$S = R^2\int_0^{2\pi}\int_0^{1+\epsilon f(\theta)} r\, dr\, d\theta = \pi R^2\left(1 + \epsilon S_1^* + \epsilon^2 S_2^*\right) \tag{21}$$

with S_1^* and S_2^* given by

$$S_1^* = \frac{1}{\pi}\int_0^{2\pi} f(\theta)\, d\theta \tag{22}$$

$$S_2^* = \frac{1}{2\pi}\int_0^{2\pi} f^2(\theta)\, d\theta \tag{23}$$

In addition to the foregoing, the perimeter (m) P is expressed by the equation

$$P = R\int_0^{2\pi}\left\{\left[1 + \epsilon f(\theta)\right]^2 + \epsilon^2 f'^2(\theta)\right\}^{1/2} d\theta = 2\pi R\left(1 + \epsilon P_1^* + \epsilon^2 P_2^* + \ldots\right) \tag{24}$$

in which

$$P_1^* = \frac{1}{2\pi}\int_0^{2\pi} f(\theta)\, d\theta = \frac{1}{2}S_1^* \quad P_2^* = \frac{1}{4\pi}\int_0^{2\pi} f'^2(\theta)\, d\theta \tag{25}$$

It is found that $S_1^* = 2P_1^*$ and $Q_1^* = 2S_1^*$.

It will be useful to establish the equations for the various results pertaining to this flow in terms of the general boundary function $f(\theta)$, before considering specific permissible forms for this function. Aside from the volumetric flow rate, the results include the average velocity across the tube $\langle v_z\rangle$ the ratio (Q/Q_c) of volumetric flow rate through the noncircular tube to that in a circular tube having the same cross-sectional area, the kinetic energy correction factor $\alpha = \langle v_z^3\rangle/\langle v_z\rangle^3$, the momentum flux coefficient $\beta = \langle v_z^2\rangle/\langle v_z\rangle^2$, the friction factor-Reynolds number relationship for the flow, and the expression for the permeability K of a packed bed based on the capillaric model comprised of these noncircular tubes. A convenient means to present these results is in terms of the quantities P_1^*, P_2^*, S_1^*, S_2^*, Q_1^*, Q_2^*, and the coefficients A_n and B_n in the series solutions for u_1 and u_2 given above. It is evident from Eqs. 13–23 that all these terms depend on the boundary function $f(\theta)$. We use the notation $\langle\Psi\rangle$ to designate the average of the quantity Ψ over the tube cross-section, given by

$$\langle\Psi\rangle = \frac{1}{S}\int_0^{2\pi}\int_0^{1+\epsilon f(\theta)}\Psi\, r\, dr\, d\theta \tag{26}$$

Average velocity and volumetric flow rate

The average velocity in the tube is given by

$$\langle v_z\rangle = \frac{R^2}{4\pi}\left(-\frac{dp}{dz}\right)\langle w\rangle = \frac{Q}{S} \approx \frac{R^2}{8\mu}\left(-\frac{dp}{dz}\right)\frac{\left(1 + \epsilon Q_1^* + \epsilon^2 Q_2^* + \ldots\right)}{\left(1 + \epsilon S_1^* + \epsilon^2 S_2^*\right)} \approx \frac{R^2}{8\mu}\left(-\frac{dp}{dz}\right) \times \left[1 + \epsilon\left(Q_1^* - S_1^*\right) + \epsilon^2\left(Q_2^* - S_1^* Q_1^* - S_1^{*2} - S_2^*\right) + O(\epsilon^3)\right]$$
$$\approx \frac{R^2}{8\mu}\left(-\frac{dp}{dz}\right)\left[1 + \epsilon S_1^* + \epsilon^2\left(Q_2^* - S_1^{*2} - S_2^*\right) + O(\epsilon^3)\right] \tag{27}$$

The volumetric flow rate for Poiseuille flow through a circular tube of cross-sectional area S is $Q_c = (S^2/8\pi\mu)(-dp/dz)$. Accordingly, for the same cross-sectional area and

pressure drop, the ratio of flow rates is given by

$$\left(\frac{Q}{Q_c}\right) \approx \frac{1+\epsilon Q_1^* + \epsilon^2 Q_2^* + \ldots}{\left(1+\epsilon S_1^* + \epsilon^2 S_2^*\right)^2} \approx 1+\epsilon\left(Q_1^* - 2S_1^*\right) + \epsilon^2\left(Q_2^* - 2S_1^* Q_1^* + 3S_1^{*2} - S_2^*\right) + \mathrm{O}(\epsilon^3) \approx 1+\epsilon^2\left(Q_2^* - S_1^{*2} - S_2^*\right) + \mathrm{O}(\epsilon^3) \quad (28)$$

We note from the expressions for Q_1^* and S_1^* in Eqs. 19 and 22 that the term of order ϵ in Eq. 28 is zero. Furthermore, the coefficient of the ϵ^2 term in this equation is always negative, demonstrating, as expected, that the volumetric flow rate for the same cross-sectional area is greatest when the boundary is circular.

Friction factor-Reynolds number relationship

The friction factor f_c for steady-state flow through the noncircular tube of length L is defined by the equation

$$f_c = \frac{SL(-dp/dz)}{PL1/2\,\rho\langle v_z\rangle^2} = \frac{r_H^2(-dp/dz)}{2\mu(Q/S)}\,\frac{16\mu}{4r_H\rho\langle v_z\rangle} = C_1\frac{16}{Re} \quad (29)$$

in which the ratio of cross-sectional area to tube perimeter is the hydraulic radius (m) $r_H = (S/P)$. The Reynolds number *Re* is defined by

$$Re = \frac{4r_H\rho\langle v_z\rangle}{\mu} = \frac{4\rho Q}{\mu P} \quad (30)$$

The geometric correction factor C_1 is given by

$$C_1 = \frac{r_H^2(-dp/dz)}{2\mu(Q/S)} = \frac{S^3(-dp/dz)}{2\mu P^2 Q} \approx \frac{\left(1+\epsilon S_1^* + \epsilon^2 S_2^*\right)^3}{\left(1+\epsilon P_1^* + \epsilon^2 P_2^* + \ldots\right)^2\left(1+\epsilon Q_1^* + \epsilon^2 Q_2^* + \ldots\right)} \approx 1+\epsilon\left(3S_1^* - 2P_1^* - Q_1^*\right) + \epsilon^2\left(3S_1^{*2} + 3S_2^* + 3P_1^{*2} + 2P_1^* Q_1^* - Q_2^* - 2P_2^* - 6P_1^* S_1^* - 3S_1^* Q_1^* + Q_1^{*2}\right) + \mathrm{O}(\epsilon^3) \approx 1+\epsilon^2\left(3S_2^* - Q_2^* - 2P_2^* + \frac{3}{4}S_1^{*2}\right) + O(\epsilon^3) \quad (31)$$

The last expression is obtained by substituting the value $P_1^* = S_1^*/2$. Again, in this case, the ϵ-term is zero, in view of the fact $Q_1^* = 2S_1^*$, and it can be shown that the ϵ^2-term is positive.

Kinetic-energy and momentum-flux correction factors

To calculate the correction factors α and β, we need to determine averages over the tube cross-section of integral powers of the velocity distribution. The power ν of the velocity distribution w, can be expressed as an expansion in ascending powers of the small parameter ϵ, which with, $x = r^2$, is given by

$$w^\nu = (1-x)^\nu\left\{1-\epsilon(1-x)^{-1}\sum_{n=0}A_n x^n\cos 2n\theta - \epsilon^2(1-x)^{-1}\sum_{n=0}B_n x^n\cos 2n\theta + \ldots\right\}^\nu \approx (1-x)^\nu - \nu\epsilon\sum_{n=0}A_n x^n(1-x)^{\nu-1}\cos 2n\theta - \epsilon^2\left[\nu\sum_{n=0}B_n x^n(1-x)^{\nu-1}\cos 2n\theta - \frac{\nu(1-\nu)}{2}\left(\sum_{n=0}A_n x^n(1-x)^{(\nu-2)/2}\cos 2n\theta\right)^2\right] + \ldots \quad (32)$$

The expansion in Eq. 32 formally accounts for all terms to $\mathrm{O}(\epsilon^2)$ in the expansion for w^ν in terms of x and θ. However, upon integration over x, from 0 to $[1+\epsilon f(\theta)]^2$, higher-order terms are introduced through the upper limit, requiring a further reordering and culling of the expansion to exclude the terms of order higher than $\mathrm{O}(\epsilon^2)$. The squared sum in the last line of Eq. 32, which could be expressed as a double summation, will reduce to a single summation upon integration over θ as all cross-product terms drop out on account of orthogonality. Using the expansion in Eq. 32, the average over the tube cross-section is calculated as follows

$$\langle w^\nu\rangle = \frac{R^2}{2S}\int_0^{2\pi}\int_0^{[1+\epsilon f(\theta)]^2} w^\nu\,dx\,d\theta \approx \frac{1}{2\left(1+\epsilon S_1^* + \epsilon^2 S_2^*\right)} \times\left\{\left[2-\nu+\frac{\nu(\nu-1)}{3}+\frac{\nu(\nu-1)(\nu-2)}{12}+\ldots\right]-2A_0\epsilon + \epsilon^2\left[\left(1-3\nu+\frac{5}{2}\nu(\nu-1)-\frac{7}{6}\nu(\nu-1)(\nu-2)+\ldots\right)\frac{1}{\pi}\int_0^{2\pi} \times f^2(\theta)\,d\theta - 2\nu\sum_{n=0}A_n\left[1-(\nu-1)+\frac{(\nu-1)(\nu-2)}{2}+\ldots\right] \times\frac{1}{\pi}\int_0^{2\pi} f(\theta)\cos 2n\theta\,d\theta - 2\nu B_0\left[1-\frac{(\nu-1)}{2}+\frac{(\nu-1)(\nu-2)}{6}+\ldots\right] + \nu(\nu-1)\left[1-\frac{(\nu-2)}{2}+\ldots\right]A_0^2 + \frac{\nu(\nu-1)}{2}\sum_{n=1}\left(\frac{1}{2n+1}-\frac{\nu-2}{2n+2}+\ldots\right)A_n^2\right]\right\} + \mathrm{O}(\epsilon^3)\,(\nu = 1, 2, \text{and } 3) \quad (33)$$

It is important to note that the terms explicitly depicted in Eq. 33 limit the expansion to calculation of $\langle w^\nu\rangle$ for only $\nu = 1$, 2 and 3; terms pertaining to $\nu \geq 4$, which are easily deduced but are unneeded, are denoted by ellipsis dots.

The averages in Eq. 33 are calculated for $\nu = 1$, 2, and 3, and the momentum and the kinetic-energy correction factors

β and α are then calculated using the equations

$$\beta = \langle w^2 \rangle / \langle w \rangle^2 \tag{34}$$

$$\alpha = \langle w^3 \rangle / \langle w \rangle^3 \tag{35}$$

Permeability based on capillaric model for packed bed

The permeability K of packed beds, having porosity ϕ, is calculated using the capillaric model of the bed, which in the present case assumes the bed is comprised of an array of the noncircular tubes. The basic relation is Darcy's Law, which relates the superficial velocity (m/s) v_0 and the pressure gradient across the bed

$$v_0 = \frac{K}{\mu}\left(-\frac{dp}{dz}\right) \tag{36}$$

In adapting the flow through the noncircular tube to the packed bed, we proceed in the same way as with calculations using the results for circular tubes. Accordingly, we identify v_0 as $\phi\langle v_z \rangle$, take the void fraction ϕ as the ratio of the total volume inside the noncircular tubes to the total volume of the bed, and determine the volume-specific surface of packing particles a_v as the ratio of the wetted surface of the tubes to the nonvoid volume. The nonvoid volume is the total bed volume less the total inside volume of the tubes. The specific surface area is also determined in terms of the mean equivalent surface and mean equivalent volume diameters of the packing particles d_s and d_v, respectively. The resulting equation for the permeability is

$$K = K_0 \frac{\left(1+\epsilon P_1^* + \epsilon^2 P_2^* + \ldots\right)^2 \left(1+\epsilon Q_1^* + \epsilon^2 Q_2^* + \ldots\right)}{\left(1+\epsilon S_1^* + \epsilon^2 S_2^*\right)^3} \tag{37}$$

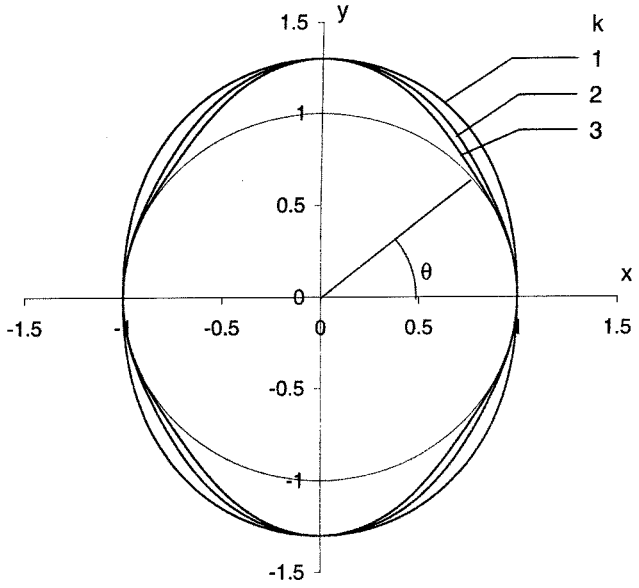

Figure 1. Capillary tube boundary: $r = 1 + \epsilon \sin^{2k}\theta$.
$k = 1, 2, 3$; $\epsilon = 0.3$.

with K_0, the permeability based on circular tubes, given by

$$K_0 = \frac{\Psi^2 d_v^2}{2(36)} \frac{\phi^3}{(1-\phi)^2} \tag{38}$$

This is the Kozeny formula for the permeability, except for the fact that the numerical factor of (2×36) in the denominator is replaced by the number 150 to account for tortuosity, among other effects. Also, $\Psi = (d_v^2/d_s^2)$ is the sphericity; d_s and d_v are the diameters of spheres having the same mean surface area, and the same mean volume, as the packing particles, respectively.

Expanded in powers of ϵ, the permeability from Eq. 37 gives

$$\begin{aligned} K &= K_0\Big[1+\epsilon(Q_1^* - 2S_1^*) \\ &\quad + \epsilon^2\left(Q_2^* - 2S_1^*Q_1^* - 3S_2^* + 2P_2^* + \frac{13}{4}S_1^{*2}\right) + O(\epsilon^3)\Big] \\ &\approx K_0\left[1+\epsilon^2\left(Q_2^* - 3S_2^* + 2P_2^* - \frac{3}{4}S_1^{*2}\right) + O(\epsilon^3)\right] \end{aligned} \tag{39}$$

where we have used $P_1^* = S_1^*/2$ in the first equality, and $Q_1^* = 2S_1^*$ in the second. We note that the ϵ-term is zero, and the ϵ^2-term is negative, as will be shown.

Boundary function $f(\theta) = \sin^{2k}\theta$ $(k = 1, 2, 3)$

The choice of boundary given by $[1+\epsilon f(\theta)] = [1+\epsilon \sin^{2k}\theta]$, with k a positive integer, embodies the required periodicity and is compatible with the symmetry requirements referred to earlier. The even power for the sine function is required to insure quadrant symmetry. Increasing the integer k for fixed ϵ increases the distortion of the pipe wall, as shown in Figure 1. The parameter ϵ may be positive or negative, albeit with small absolute value. Our calculations are first aimed at determining the values of the coefficients A_n and B_n in the series solutions for $u_1(r,\theta)$ and $u_2(r,\theta)$, Eqs. 12 and 15, and the terms Q_1^*, Q_2^*, S_1^*, S_2^*, P_1^* and P_2^*. These are then used to calculate the various results presented in the foregoing. Calculations are carried out for $k = 1$, 2, and 3. The general formulas for the needed trigonometric integrals are given by Gradshteyn and Ryzhik (1965), although we note here that we rederived these integrals as corrections were necessary in some cases.

It is a straightforward matter to show that all of the needed results can be calculated through appropriate adaptation of two integral formulas. The first formula is (Gradshteyn and Ryzhik (1965), No. 3.621-3, p. 369)

$$\int_0^{2\pi} \sin^{2k}\theta\, d\theta = 2\pi \frac{(2k-1)!!}{(2k)!!} \tag{40}$$

in which the following notation is used

$$(2k-1)!! \equiv 1.3\ldots(2k-1) \tag{41}$$

$$(2k)!! \equiv 2.4\ldots(2k) \tag{42}$$

The second integral formula is (Gradshteyn and Ryzhik, 1965,

Table 1. Values of A_n for $f(\theta) = \sin^{2k}\theta$ (Eqs. 13 and 14)

k	A_0	A_1	A_2	A_3	A_4
1	−1	1	0	0	0
2	−3/4	1	−1/4	0	0
3	−5/8	15/16	−3/8	1/16	0

p. 373)

$$\int_0^{2\pi} \sin^{2k}\theta \cos 2n\theta \, d\theta = 2\pi \frac{(-1)^n}{2^{2k}} \Xi[2k/(k-n)] \quad \text{for } k \geq n$$

$$= 0 \quad \text{for } k < n \qquad (43)$$

which employs the following notation

$$\Xi[p/m] \equiv \frac{p(p-1)\ldots(p-m+1)}{1.2\ldots m}; \quad \Xi[p/0] = 1 \qquad (44)$$

We note that the integrals containing the product ($\cos 2n\theta \cos 2m\theta$) in Eq. 17 for the constants B_n can be evaluated using the formula in Eq. 43 after the product of cosines is reexpressed in terms of the cosines of the sum and difference of the angles.

To facilitate calculation of all results pertaining to the flow which were presented in preceding sections, tables of integrals over θ from 0 to 2π were calculated, in which $f(\theta) = \sin^{2k}\theta$ ($k = 1, 2, 3$) for the following integrands: $f(\theta)$, $f^2(\theta)$, $f(\theta) \cos 2n\theta$, $f^2(\theta) \cos 2n\theta$, and $f(\theta)\cos 2n\theta \cos 2m\theta$. These are given in the Appendix.

Coefficients in velocity expansion for $f(\theta) = \sin^{2k}\theta$ ($k = 1, 2, 3$)

The coefficients A_n in the series solution for the term $u_1(r, \theta)$ in the asymptotic expansion Eq. 7 for the dimensionless velocity distribution $u(r, \theta)$ are defined by Eqs. 13 and 14. The calculated values of A_n, using the tabulated integrals given in the Appendix are given in Table 1, from which it is observed that the series solution for $u_1(r, \theta)$ has only a few nonzero terms, depending on the value of the exponent k.

The coefficients B_n in the series solution for the term $u_2(r, \theta)$ in the asymptotic expansion Eq. 7 for $u(r, \theta)$ are defined by Eqs. 16 and 17. The calculated values of B_n are given in Table 2. It is observed again that the series solution for $u_2(r, \theta)$ also has only a few nonzero terms, albeit more terms for each k than the series for $u_1(r, \theta)$.

The finding that the series representations for the terms in the expansion for $u(r, \theta)$ only have a few nonzero terms makes calculation of results quite convenient, and permits one to determine all the terms complete to the appropriate order of approximation, which in this work is to order ϵ^2, inclusive. Aside from the coefficients A_n and B_n, we need to calculate the terms P_1^*, P_2^*, S_1^*, S_2^*, Q_1^*, and Q_2^* from the relationships in Eqs. 19–25 for $f(\theta) = \sin^{2k}\theta$. These are determined using the tabulated integrals in the Appendix. The values of these terms are given in Table 3.

Table 3. Values of P_1^*, P_2^*, S_1^*, S_2^*, Q_1^* and Q_2^* for $f(\theta) = \sin^{2k}\theta$ (Eqs. 19–25)

k	P_1^*	P_2^*	S_1^*	S_2^*	Q_1^*	Q_2^*
1	1/2	1/4	1	3/8	2	5/4
2	3/8	5/16	3/4	35/128	3/2	33/64
3	5/16	189/512	5/8	231/1,024	5/4	93/512

The tube perimeter P, cross-sectional area S, and the volume rate of flow Q are given by Eqs. 25, 21, and 18, respectively, using the terms in Table 3.

The average velocity $\langle v_z \rangle$ from Eq. 27, and the volumetric flow rate ratio (Q/Q_c), given by Eq. 28, were calculated for the boundary function $f(\theta) = \sin^{2k}\theta$ for $k = 1$, 2, and 3. The results are given in Table 4.

It is found that the ratio of volumetric flow rates (Q/Q_c) is less than 1, since as expected the volumetric flow rate for the same cross-sectional area and pressure drop is greatest when the boundary is a circular. Also, using the results from Table 4, we find the ratio $[2\langle v_z \rangle / v_{z\max}] = 1 - C\epsilon^2 + \ldots$, with $C = 0$ for $k = 1$, $C = (1/32)$ for $k = 2$, and $C = (19/256)$ for $k = 3$.

The friction factor-Reynolds number and the permeability geometric factors C_1 given by Eq. 31, and (K/K_0) given by Eq. 39, are listed in Table 5 for the boundary function for $f(\theta) = \sin^{2k}\theta$ for $k = 1$, 2, and 3.

The results in Table 5 demonstrate that the friction factor geometric factor is larger than 1, and that the permeability is smaller in the noncircular tube, and the effects are indifferent to whether ϵ is positive or negative, as required.

The momentum flux and kinetic-energy correction factors β and α from Eqs. 34 and 35 for $f(\theta) = \sin^{2k}\theta$ are given in Table 6.

It is evident that both correction factors α and β are the same as those for a circular boundary up to, and including, the ϵ^2-term for $k = 1$. In addition, for $k > 1$, these factors are larger than the corresponding correction factors for the circular boundary; the $O(\epsilon)$ terms are zero, whereas the $O(\epsilon^2)$ terms are positive and increase with increasing k.

Capillary Flow through the Noncircular Tube

The results in the foregoing are now applied to calculate the capillary rise in the noncircular tube. The driving force for the capillary rise in a circular tube of radius (m) R is given by

$$\Delta p = (2\sigma \cos\theta_c / R) - \rho g h \qquad (45)$$

Table 2. Values of B_n for $f(\theta) = \sin^{2k}\theta$ (Eqs. 16 and 17)

k	B_0	B_1	B_2	B_3	B_4	B_5	B_6	B_7
1	1/8	−1/2	3/8	0	0	0	0	0
2	37/128	−11/16	21/32	−5/16	7/128	0	0	0
3	369/1,024	−201/256	1,065/2,048	−275/512	231/1,024	−27/512	11/2,048	0

Table 4. Average and Maximum Velocity and (Q/Q_c) for $f(\theta)=\sin^{2k}\theta$ (Eqs. 27 and 28)

k	$\langle v_z\rangle/[(R^2/8\mu)(-dp/dz)]$	$v_{z\max}/[(R^2/4\mu)(-dp/dz)]$	(Q/Q_c)
1	$1+\epsilon-(1/8)\epsilon^2+\ldots$	$1+\epsilon-(1/8)\epsilon^2+\ldots$	$1-(1/8)\epsilon^2+\ldots$
2	$1+(3/4)\epsilon-(41/128)\epsilon^2+\ldots$	$1+(3/4)\epsilon-(37/128)\epsilon^2+\ldots$	$1-(41/128)\epsilon^2+\ldots$
1	$1+(5/8)\epsilon-(445/1{,}024)\epsilon^2+\ldots$	$1+(5/8)\epsilon-(369/1{,}024)\epsilon^2+\ldots$	$1-(445/1{,}024)\epsilon^2+\ldots$

in which σ is the surface tension (N/m), θ_c is the contact angle, and h is the height of the liquid column in the tube at time t. In Eq. 45 the first term on the lefthand side is the capillary pressure, the radius of curvature being taken as the radius of the tube since the meniscus is assumed to be part spherical. The second term is the hydrostatic pressure. The equilibrium height of liquid in a tube open to the atmosphere above a reservoir of the liquid, also open to the atmosphere, is attained when the capillary pressure equals the hydrostatic pressure, and is given by

$$h_{\infty c}=(2\sigma\cos\theta_c/\rho gR) \tag{46}$$

The problem of the capillary flow of a liquid in a circular tube was treated theoretically nearly eight decades ago by Washburn (1921); the theory is sometimes referred to as the Washburn-Rideal-Lucas (WRL) result (Joos et al., 1990). Washburn combined Poiseuille's law for the average velocity for the laminar flow in a circular tube with the pressure drop given by Eq. 45 to get the equation for the rate of change of the height of liquid in the capillary, given by

$$\frac{dh}{dt}=\frac{\sigma R}{4\mu h}\cos\theta_c-\frac{\rho gR^2}{8\mu} \tag{47}$$

Equation 47 is transformed to the form

$$\cos\theta_c\frac{d\chi}{d\tau}\frac{1}{H^2}\left(\frac{1}{\chi}-1\right) \tag{48}$$

in which we have used the dimensionless variables

$$\tau=(4\sigma t/\mu R),\ \chi=h/[2\sigma\cos\theta_c/\rho gR],\ H=(8\sigma/\rho gR^2) \tag{49}$$

Table 5. Friction Factor and Permeability Geometric Factors for $f(\theta)=\sin^{2k}\theta$

k	$C_1=(f_c Re/16)$	(K/K_0)
1	$1+(1/8)\epsilon^2+\ldots$	$1-(1/8)\epsilon^2+\ldots$
2	$1+(13/128)\epsilon^2+\ldots$	$1-(13/128)\epsilon^2+\ldots$
3	$1+(51/1{,}024)\epsilon^2+\ldots$	$1-(51/1{,}024)\epsilon^2+\ldots$

Table 6. Correction Factors β and α for $f(\theta)=\sin^{2k}\theta$ (Eqs. 35 and 36)

k	$\beta=\langle w^2\rangle/\langle w\rangle^2$	$\alpha=\langle w^3\rangle/\langle w\rangle^3$
1	$(4/3)+O(\epsilon^3)$	$2+O(\epsilon^3)$
2	$(4/3)+(1/40)\epsilon^2+\ldots$	$2+(7/80)\epsilon^2+\ldots$
3	$(4/3)+(403/6{,}720)\epsilon^2\ldots$	$2+(3{,}753/17{,}920)\epsilon^2+\ldots$

Integration of Eq. 48 between the limits $\chi(0)=0$ and $\chi(\tau)$ then gives the WRL equation

$$(\tau/H^2)=-\cos\theta_c[\chi+\ln(1-\chi)] \tag{50}$$

In extending the WRL analysis to the noncircular tube considered here, we use the average velocity from Eq. 27 for (dh/dt), with the pressure gradient taken as $(\Delta p/h)$. As with Eq. 45, the pressure drop consists of the capillary pressure and the hydrostatic pressure terms, except that we use the hydraulic radius $r_H=(S/P)$ in place of $(R/2)$ in the former (Mason and Morrow, 1991; Kim and Whitesides, 1997). Accordingly

$$\Delta p=(\sigma\cos\theta_c/r_H)-\rho gh \tag{51}$$

Using Eqs. 21, 24 and 27, we get

$$\begin{aligned}\frac{dh}{dt}&=\frac{R^2}{8\mu h}\frac{(1+\epsilon Q_1^*+\epsilon^2Q_2^*+\ldots)}{(1+\epsilon S_1^*+\epsilon^2S_2^*)}\left[\frac{\sigma\cos\theta_c}{r_H}-\rho gh\right]\\&\approx\frac{R^2}{8\mu h}\frac{(1+\epsilon Q_1^*+\epsilon^2Q_2^*+\ldots)}{(1+\epsilon S_1^*+\epsilon^2S_2^*)}\\&\quad\times\left[\frac{2\sigma\cos\theta_c}{R}\frac{(1+\epsilon P_1^*+\epsilon^2P_2^*+\ldots)}{(1+\epsilon S_1^*+\epsilon^2S_2^*)}-\rho gh\right]\\&\approx\frac{\sigma R\cos\theta_c}{4\mu h}D(\epsilon)-\frac{\sigma gR^2}{8\mu}E(\epsilon)\end{aligned} \tag{52}$$

When Eq. 52 is written in terms of the dimensionless variables 49, we get

$$\cos\theta_c\frac{d\chi}{d\tau}\approx\frac{1}{H^2}\left[\frac{D(\epsilon)}{\chi}-E(\epsilon)\right] \tag{53}$$

with

$$\begin{aligned}D(\epsilon)&\approx\frac{(1+\epsilon Q_1^*+\epsilon^2Q_2^*+\ldots)(1+\epsilon P_1^*+\epsilon^2P_2^*+\ldots)}{(1+\epsilon S_1^*+\epsilon^2S_2^*)^2}\approx1\\&\quad+\frac{1}{2}\epsilon S_1^*+\epsilon^2(Q_2^*+P_2^*-2S_2^*-S_1^{*2})+\ldots\end{aligned} \tag{54}$$

$$\begin{aligned}E(\epsilon)&\approx\frac{(1+\epsilon Q_1^*+\epsilon^2Q_2^*+\ldots)}{(1+\epsilon S_1^*+\epsilon^2S_2^*)}\approx1+\epsilon S_1^*\\&\quad+\epsilon^2(Q_2^*-S_2^*-S_1^{*2})+\ldots\end{aligned} \tag{55}$$

The expressions for $D(\epsilon)$ and $E(\epsilon)$ are based on using the fact that $Q_1^*=2S_1^*$ and $P_1^*=(1/2)\ S_1^*$.

Table 7. χ_∞ and Ratio ($h_\infty/h_{\infty c}$) for Fixed S for $f(\theta)=\sin^{2k}\theta$ (Eqs. 57 and 58)

k	$\chi_\infty \approx 1-(1/2)\epsilon S_1^* + \epsilon^2[P_2^* - S_2^* + (1/2)S_1^{*2}] + \ldots$	$(h_\infty/h_{\infty c}) \approx 1+\epsilon^2[P_2^* - (1/2)S_2^* + (1/8)S_1^{*2}] + \ldots$
1	$1-(1/2)\epsilon+(3/8)\epsilon^2+\ldots$	$1+(3/16)\epsilon^2+\ldots$
2	$1-(3/8)\epsilon+(41/128)\epsilon^2+\ldots$	$1+(69/256)\epsilon^2+\ldots$
3	$1-(5/16)\epsilon+(347/1{,}024)\epsilon^2+\ldots$	$1+(625/2{,}048)\epsilon^2+\ldots$

Integration of Eq. 53 between the limits $\chi(0)=0$ and $\chi(\tau)$ then gives

$$\frac{\tau}{H^2\cos\theta_c} \approx -\frac{D(\epsilon)}{E^2(\epsilon)}\left\{\frac{\chi}{\chi_\infty}+\ln\left[1-\frac{\chi}{\chi_\infty}\right]\right\} \qquad (56)$$

in which we have used the fact that the equilibrium height of liquid χ_∞, obtained from Eq. 53 upon setting $d\chi/d\tau=0$, is given by

$$\chi_\infty \approx \frac{h_\infty}{(2\sigma\cos\theta_c/\rho g R)} \approx \frac{D(\epsilon)}{E(\epsilon)} \approx 1-\frac{1}{2}\epsilon S_1^* + \epsilon^2\left(P_2^* - S_2^* + \frac{1}{2}S_1^{*2}\right)+\ldots \qquad (57)$$

When we set $\epsilon=0$ in Eq. 56, the WRL result is obtained. Equation 56 can be used to construct plots of the dependence $\chi=\chi(\tau;\ \epsilon)$ using the values for $D(\epsilon)$ and $E(\epsilon)$ from Eqs. 54 and 55. We recognize that the relationship depicted by Eq. 56 is strictly correct to terms of $O(\epsilon^2)$ in conformance with the order of approximation pertaining to $D(\epsilon)$ and $E(\epsilon)$.

Equation 57 may give the illusion that the equilibrium height of liquid in the noncircular tube is smaller or larger than that in the circular tube depending upon whether the parameter ϵ is positive or negative, respectively. However, this is only due to the fact that Eq. 57 does not give the equilibrium height of liquid relative to the same basis in the two cases; the cross-sectional areas of the flows are different in the two cases. A proper reference for expressing the equilibrium height of liquid would be on the basis of equal cross-sectional areas (m^2) S of circular and noncircular tubes. In terms of the area S, the equilibrium height is given by

$$h_\infty \approx \frac{2\sigma\cos\theta_c}{\rho g\sqrt{S/\pi}}\left\{\left(1+\epsilon P_1^*+\epsilon^2 P_2^*+\ldots\right)\left(1+\epsilon S_1^*+\epsilon^2 S_2^*\right)^{-1/2}\right\} \approx \frac{2\sigma\cos\theta_c}{\rho g\sqrt{S/\pi}}\left\{1+\epsilon^2\left(P_2^*-\frac{1}{2}S_2^*+\frac{1}{8}S_1^{*2}\right)+\ldots\right\} \qquad (58)$$

It is obvious that the ratio of heights of liquid in noncircular to circular tubes having the same cross-sectional areas is given by the term in brackets in Eq. 58. Values of χ_∞ from Eq. 57, and the ratio of heights ($h_\infty/h_{\infty c}$) from Eq. 58 for the boundary function $f(\theta)=\sin^{2k}\theta$ are given in Table 7, from which it is evident that the penetration of liquid is deeper for the noncircular tube. Furthermore, it increases as the value of k increases irrespective of the sign of ϵ. It needs to be observed that while geometric similarity in boundary shape is not preserved as k is changed, the mean radius of curvature decreases as k increases, and the trend predicted from Eq. 58 is as expected.

Equation 56 can be used to compare capillary rise curves for different values of the boundary function coefficient k. However, plots of (χ/χ_∞) against τ for different values of k and ϵ would pertain to tubes of different cross-sectional areas. A proper comparison requires that variables are normalized to the same cross-section for flow. This is done by redefining the variable τ and the parameter H, given in Eq. 49, in terms of the area S instead of R. Equation 21 relating S and R is used with Eq. 49 to get

$$\tau_s = \frac{4\sigma t}{\mu\sqrt{S/\pi}}\frac{(\rho g S/\pi)^2}{(8\sigma)^2}\frac{1}{\cos\theta_c} = \left(1+\epsilon S_1^*+\epsilon^2 S_2^*\right)^{3/2}\left(\frac{\tau}{H^2\cos\theta_c}\right) \qquad (59)$$

When Eq. 59 is combined with Eq. 56, we get

$$\tau_s \approx \left[1+\epsilon^2\left(P_2^*-Q_2^*+\frac{3}{2}S_2^*+\frac{9}{8}S_1^{*2}\right)+\ldots\right]\times\left[\frac{\chi}{\chi_\infty}+\ln\left(1-\frac{\chi}{\chi_\infty}\right)\right] \qquad (60)$$

The variables τ_s and (χ/χ_∞) are normalized to fixed cross-sectional area regardless of boundary shape. Figure 2 depicts the capillary rise curves using Eq. 60. The coefficient of the ϵ^2-term in Eq. 60 is always positive, and takes on the progressively increasing values (11/16), (215/256) through (1977/2048) as the boundary function coefficient k increases from 1 to 2 to 3. It is clear from Figure 2 that the penetration rate is increasingly retarded as the boundary shape progressively departs from the circular shape. However, we need to observe that, for the choice of function $f(\theta)=\sin^{2k}\theta$, the boundary shapes do not change significantly as k increases from 1 to 3, as can be surmised from Figure 1. Consequently, the capillary rise curves for any given value of ϵ, when normalized to constant cross-sectional area, tend to be quite close. The effects of large variations in boundary shape are examined in the next section.

Results for the Boundary Function $f(\theta)=\sin^2 k\theta$

The boundary defined by $r=1+\epsilon\ \sin^2 k\theta$, with k a positive integer, is useful, because it provides broad choices of shapes through variation of the magnitude of ϵ and the value of k, which, as shown in Figure 3, include an approximation to a square shape, evolving into the corrugated tube as k increases. Clearly, the ranges of the approximations, being asymptotic expansions in ϵ, will be circumscribed by the value of k; the larger the value of k, the smaller ϵ must be to preserve the asymptotic nature of the expansions.

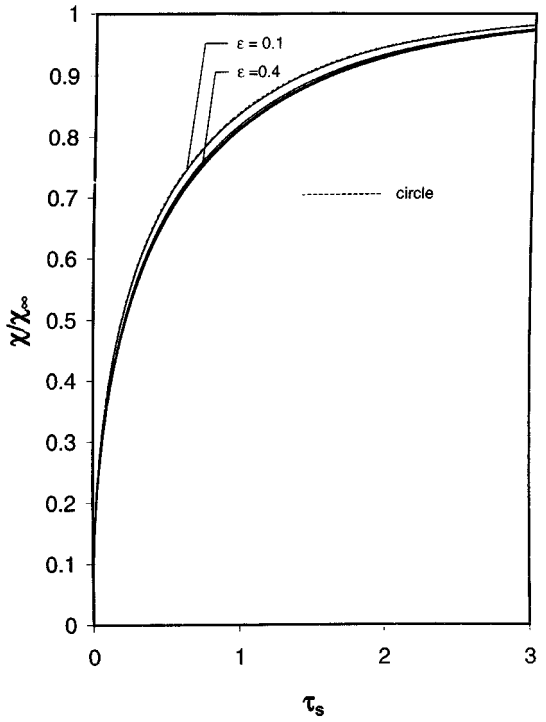

Figure 2. Capillary rise curve (Eq. 60), for tube boundary $r = 1 + \epsilon \sin^{2k}\theta$.

$k = 1, 2, 3$; $\epsilon = 0.2$.

All the results obtained above in terms of $f(\theta)$, in general form, can be specialized for this case, and expressed by equations in terms of k and ϵ. The coefficients A_n and B_n in the series solutions for $u_1(r, \theta)$ and $u_2(r, \theta)$, given by Eqs. 12 and 15, are given by

$$A_n(k) = -\delta_{n0} + \delta_{nk} \tag{61}$$

$$B_n(k) = \left(\frac{1}{2}k - \frac{3}{8}\right)\delta_{n0} - \left(k - \frac{1}{2}\right)\delta_{nk} + \left(\frac{1}{2}k - \frac{1}{8}\right)\delta_{n(2k)} \tag{62}$$

in which, as usual, the Kronecker delta $\delta_{ij} = 1$ when $i = j$ and $\delta_{ij} = 0$ otherwise. It is evident from the results here, and those presented earlier, that the symmetry requirements imposed on the flow at the outset lead to significant simplification of the analysis, without detracting from their broad value.

The expansion coefficients for the perimeter P (Eq. 25), area S (Eqs. 22–23) and the volumetric flow rate (m^3/s) Q (Eqs. 19–20) are given in Table 8 as functions of k.

All results derived above for the boundary function $f(\theta)$, in general form, can be specialized for the case $f(\theta) = \sin^2 k\theta$, using the values in Table 8 and Eqs. 61 and 62. The principal results pertaining to this choice of boundary function are presented in Table 9 as expressions in terms of k and ϵ. It is obvious from Figure 3, which depicts boundary shape corresponding to $f(\theta) = \sin^2 k\theta$, that increasing the integral value

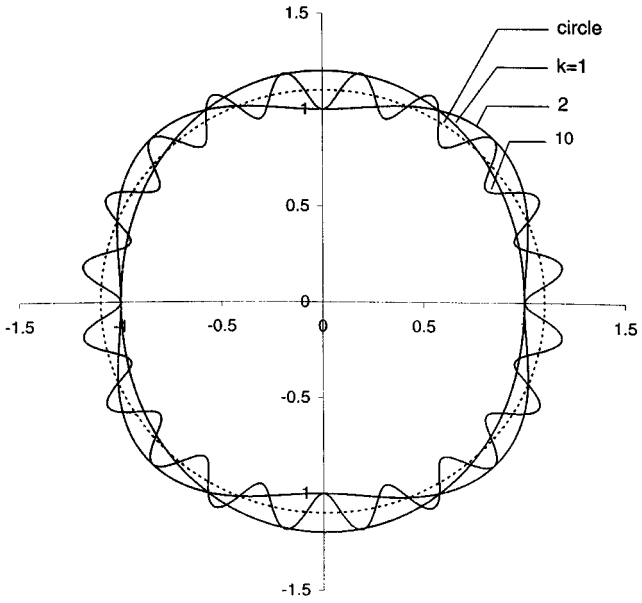

Figure 3. Capillary tube boundary: $r = 1 + \epsilon \sin^2 k\theta$.

$k = 1, 2, 10$; $\epsilon = 0.3$.

Table 8. Values of P_1^*, P_2^*, S_1^*, S_2^*, Q_1^* and Q_2^* for $f(\theta) = \sin^2 k\theta$ (Eqs. 19–25)

P_1^*	P_2^*	S_1^*	S_2^*	Q_1^*	Q_2^*
1/2	$k^2/4$	1	3/8	2	$(9/4) - k$

Table 9. Flow Properties for Boundary Function $f(\theta) = \sin^2 k\theta$

(1)	$\langle v_z\rangle / \left[\frac{R^2}{8\mu}\left(-\frac{dp}{dz}\right)\right]$	$\approx 1 + \epsilon - \frac{(8k-7)}{8}\epsilon^2 + \ldots$	(27)
(2)	$v_{z\max} / \left[\frac{R^2}{4\mu}\left(-\frac{dp}{dz}\right)\right]$	$\approx 1 + \epsilon - \frac{(4k-3)}{8}\epsilon^2 + \ldots$	
(3)	$2\langle v_z\rangle / [v_{z\max}]$	$\approx 1 - \frac{(k-1)}{2}\epsilon^2 + \ldots$	
(4)	(Q/Q_c)	$\approx 1 - \frac{(8k-7)}{8}\epsilon^2 + \ldots$	(28)
(5)	$C_1 = (16 f_c/Re)$	$\approx 1 - \frac{(2k-1)(2k-3)}{8}\epsilon^2 + \ldots$	(31)
(6)	(K/K_0)	$\approx 1 + \frac{(2k-1)(2k-3)}{8}\epsilon^2 + \ldots$	(39)
(7)	$\beta = \langle w^2\rangle / \langle w\rangle^2$	$\approx \frac{4}{3} + \frac{2(k-1)(2k-1)}{3(2k+1)}\epsilon^2 + \ldots$	(34)
(8)	$\alpha = \langle w^3\rangle / \langle w\rangle^3$	$\approx 2 + \frac{(k-1)(2k-1)(2k+3)}{(k+1)(2k+1)}\epsilon^2 + \ldots$	(35)
(9)	$D(\epsilon)/E^2(\epsilon)$	$\approx 1 - \frac{3}{2}\epsilon + \frac{(k+1)(k+3)}{4}\epsilon^2 + \ldots$	(56)
(10)	χ_∞	$\approx 1 - \frac{1}{2}\epsilon + \frac{(2k^2+1)}{8}\epsilon^2 + \ldots$	(57)
(11)	$(h_\infty/h_{\infty c})$	$\approx 1 + \frac{(2k-1)(2k+1)}{16}\epsilon^2 + \ldots$	(58)
(12)	τ_s	$\approx -\left[1 + \frac{(2k-1)(2k+9)}{16}\epsilon^2 + \ldots\right] \times \left[\frac{\chi}{\chi_\infty} + \ln\left(1 - \frac{\chi}{\chi_\infty}\right)\right]$	(60)

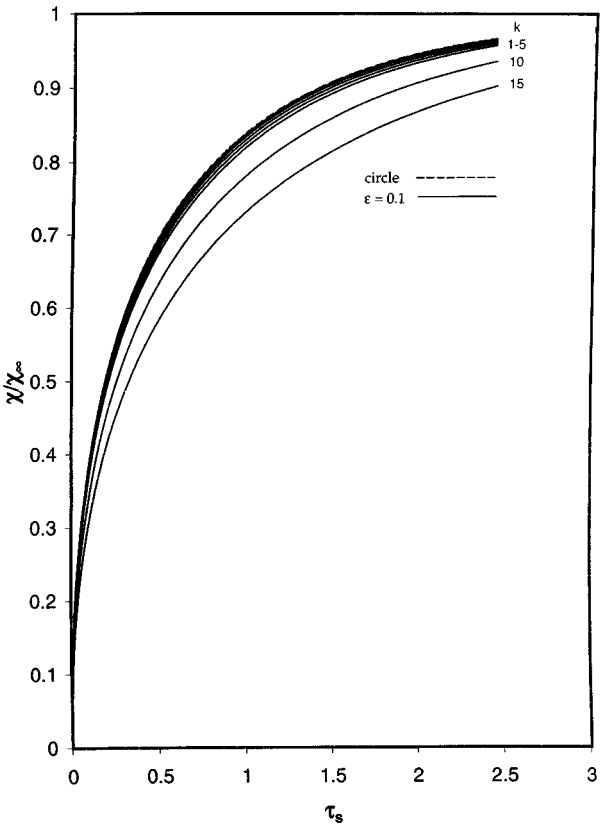

Figure 4. Capillary rise curve (Eq. 60) (Table 9, No. 12) for tube boundary $r = 1 + \epsilon \sin^2 k\theta$.

$k = 1, 2, 3, 4, 5, 10, 15$; $\epsilon = 0.1$.

of k results in significant change in boundary geometry, and the expressions in Table 9 suggest that the resulting effect on flow properties is also significant. Plots of (χ/χ_∞) against τ_s using expansion No. 12 from Table 9 are given in Figure 4, which demonstrates that tube geometry strongly affects the rate of capillary flow. In particular, the plots in Figure 4 indicate that, based on equal cross-sectional area, the penetration rate is increasingly retarded the further the departure from the circular shape (k increasing). Furthermore, the results in Table 7, as well as expansion No. 11 in Table 9, for the ratio $(h_\infty/h_{\infty c})$, demonstrate that the penetration in the noncircular tube is deeper than that for a circular tube of the same cross-sectional area. These results are consistent with the fact that the mean curvature, which is proportional to the ratio (P/S), increases for fixed S the further the boundary departs from the circular shape.

Conclusions

The principal guideline governing the choice of problem, and associated analysis, presented in the foregoing was to establish a framework in which the role of tube geometry on flow properties could be probed in a direct way. Accordingly, explicit analytical results for all flow properties are derived in which the role of boundary shape is articulated directly in terms of the function $f(\theta)$, in general form, as well as for the specific choices $f(\theta) = \sin^{2k}\theta$ ($k = 1$, 2, and 3), and for $f(\theta) = \sin^2 k\theta$ with k a positive integer. The choice of $f(\theta)$ permits one to change boundary shape, and the choice of the value of the parameter ϵ permits one to determine the degree of the change. Aside from these, an additional attribute of the analysis here resides in the fact that each result for the noncircular tube is established relative to the corresponding flow property for the circular tube as the reference. The results in terms of the general form of $f(\theta)$ are complete with all relevant flow properties expressed in terms of dimensionless factors pertaining to tube geometry and volumetric flow rate (that is, P_1^*, P_2^*, S_1^*, S_2^*, Q_1^* and Q_2^*). Accordingly, extension of the calculations to other permissible choices of the boundary-shape function is straightforward. The variety of admissible boundary-shape functions is broad, and includes, for example, $f(\theta) = \sin^{2k}\theta + \cos^{2k}\theta$, which through choice of k and ϵ can provide a boundary approximating a square with rounded corners, or one with concave and convex surfaces. This function can be reduced to a polynomial in $\sin^{2k}\theta$, of degree k or $(k-1)$, depending upon whether k is an even or an odd integer, respectively. Therefore, the results for this function, which represents a superposition of the shape corresponding to $\sin^{2k}\theta$ upon that of its rotation through 90 degrees, can be constructed directly using the trigonometric integrals given here. It is clear from the overall results obtained here that boundary geometry has a strong effect on capillary flow.

Acknowledgment

Professor Alkis Payatakes of the University of Patras and his PhD students, Drs. Dimitris Avraam and Christos Tsakiroglou, were very kind to provide me (RMT) with a detailed list of literature sources on the subject in this article. My interest in this subject, and many of the ideas in this article, have received reinforcement and inspiration through my many interactions with Alkis Payatakes, Raj Rajagopalan of Florida, Hemant Pendse of Maine and, most especially, Chi Tien of Syracuse.

Notation

h = height of capillary rise, m
h_∞ = equilibrium height of capillary rise, m
p = pressure, Pa
P_1^*, P_2^* = dimensionless expansion coefficients for P, Eq. 24
Q_1^*, Q_2^* = dimensionless expansion coefficients for Q, Eq. 18
r = dimensionless radial coordinate
S_1^*, S_2^* = dimensionless expansion coefficients for S, Eq.. 21
$u(r, \theta) = (1 - r^2) - w(r, \theta)$, reduced dimensionless velocity
v_z = axial velocity in tube, m/s
$w(r\theta) = v_z/[R^2(-dp/dz)/4\mu]$, dimensionless axial velocity
$x = r^2$
μ = viscosity, Pa·s
ρ = density, kg/m^3
ϕ = void fraction in packed bed
$\chi = h/[2\sigma \cos \theta_c/\rho g R]$, dimensionless capillary rise, Eq. 49
$\chi_\infty = h_\infty/[2\sigma \cos \theta_c/\rho g R]$

Literature Cited

Bracke, M., F. DeBisschop, and P. Joos, "Contact Angle Hysteresis Due to Surface Roughness," *Prog. Colloid Poly. Sci.*, **76**, 251 (1988).

Bracke, M., F. de Veoght, and P. Joos, "The Kinetics of Wetting: the Dynamic Contact Angle," *Prog. Colloid Poly. Sci.*, **79**, 142 (1989).

Dryden, H. L., F. D. Murnaghan, and H. Bateman, *Hydrodynamics*, Dover, New York (1956).

Gradshteyn, I. S., and I. M. Ryzhik, *Table of Integrals, Series, and Products*, Academic Press, New York (1965).

Huisman, H. F., "Contact Angle and the Rootare-Prenzlow Equation in Mercury Intrusion Porosimetry," *J. Colloid Interface Sci.*, **94**, 25 (1983).
Joos, P., P. V. Remoortere, and M. Bracke, "The Kinetics of Wetting in a Capillary," *J. Colloid Interface Sci.*, **136**, 189 (1990).
Kim, E., and G. M. Whitesides, "Imbibition and Flow of Wetting Liquids in Noncircular Capillaries," *J. Phys. Chem. B*, **101**, 855 (1997).
Langlois, W. E., *Slow Viscous Flow*, Macmillan, New York (1964).
Marmur, A., "The Radial Capillary," *J. Colloid Interface Sci.*, **124**, 301 (1988).
Mason, G., and N. R. Morrow, "Capillary Behavior of a Perfectly Wetting Liquid in Irregular Triangular Tubes," *J. Colloid Interface Sci.*, **141**, 262 (1991).
Mason, G., and N. R. Morrow, "Effect of Contact Angle on Capillary Displacement Curvatures in Pore Throats Formed by Spheres," *J. Colloid Interface Sci.*, **168**, 130 (1994).
Mason, G., M. D. Nguyen, and N. R. Morrow, "Effect of Contact Angle on the Meniscus between Two Equal Contacting Rods and a Plate," *J. Colloid Interface Sci.*, **95**, 494 (1983).
Mayer, R. P., and R. A. Stowe, "Mercury Porosimetry-Breakthrough Pressure for Penetration-Between Packed Spheres," *J. Colloid Sci.*, **20**, 893 (1965).
Princen, H. M., "Capillary Phenomena in Assemblies of Parallel Cylinders: I. Capillary Rise between Two Cylinders," *J. Colloid Interface Sci.*, **30**, 69 (1969a).
Princen, H. M., "Capillary Phenomena in Assemblies of Parallel Cylinders: II. Capillary Rise in Systems with More Than Two Cylinders," *J. Colloid Interface Sci.*, **30**, 359 (1969b).
Princen, H. M., "Capillary Phenomena in Assemblies of Parallel Cylinders: III. Liquid Columns between Horizontal Parallel Cylinders," *J. Colloid Interface Sci.*, **34**, 171 (1970).
Remoortere, P. V., and P. Joos, "The Kinetics of Wetting: The Motion of a Three Phase Contactline in a Capillary," *J. Colloid Interface Sci.*, **141**, 348 (1991).
Remoortere, P. V., and P. Joos, "About the Kinetics of Partial Wetting," *J. Colloid Interface Sci.*, **160**, 387 (1993).
Rillaerts, E., and P. Joos, "The Dynamic Contact Angle," *Chem. Eng. Sci.*, **35**, 883 (1980).
Shah, R. K., and A. L. London, *Advances in HEAT TRANSFER: Supplement 1: Laminar Flow Forced Convection in Ducts*, Academic Press, New York (1978).
Smith, D. M., and D. L. Stermer, "Mercury Porosimetry: Theoretical and Experimental Characterization of Random Microsphere Packings," *J. Colloid Interface Sci.*, **111**, 160 (1986).
Snyder, W. T., and G. A. Goldstein, "An Analysis of Fully Developed Laminar Flow in an Eccentric Annulus," *AIChE J.*, **11**, 462 (1965).
Washburn, E. W., "The Dynamics of Capillary Flow," *Phys. Rev.*, **17**, 273 (1921).

Appendix: Selected Trigonometric Integrals

The tables of trigonometric integrals in this section were calculated using the formulas in Eqs. 40–44.

Table A1. Integrals of $f(\theta)\cos 2n\theta$ and $f^2(\theta)\cos 2n\theta$

	$\frac{1}{\pi}\int_0^{2\pi}\sin^{2k}\theta\cos 2n\theta\,d\theta$			$\frac{1}{\pi}\int_0^{2\pi}\sin^{4k}\theta\cos 2n\theta\,d\theta$		
n	$k=1$	$k=2$	$k=3$	$k=1$	$k=2$	$k=3$
0	1	3/4	5/8	3/4	35/64	231/512
1	−1/2	−1/2	−15/32	−1/2	−7/16	−99/256
2	0	1/8	3/16	1/8	7/32	495/2,048
3		0	−1/32	0	−1/16	−55/512
4			0		1/128	33/1,024
5					0	−3/512
6						1/2,048
7						0

Table A2a. $\frac{1}{\pi}\int_0^{2\pi}\sin^{2k}\theta\cos 2n\theta\cos 2m\theta\,d\theta$ $(k=1)$

m/n	0	1	2	3	4	5	6
0	**1**	−1/2	0				
1	−1/2	**1/2**	−1/4	0			
2	0	−1/4	**1/2**	−1/4	0		
3		0	−1/4	**1/2**	−1/4	0	
4			0	−1/4	**1/2**	−1/4	0

Table A2b. $\frac{1}{\pi}\int_0^{2\pi}\sin^{2k}\theta\cos 2n\theta\cos 2m\theta\,d\theta$ $(k=2)$

m/n	0	1	2	3	4	5	6	7	8
0	**3/4**	−1/2	1/8	0					
1	−1/2	**7/16**	−1/4	1/16	0				
2	1/8	−1/4	**3/8**	−1/4	1/16	0			
3	0	1/16	−1/4	**3/8**	−1/4	1/16	0		
4		0	1/16	−1/4	**3/8**	−1/4	1/16	0	
5			0	1/16	−1/4	**3/8**	−1/4	1/16	0

Table A2c. $\frac{1}{\pi}\int_0^{2\pi}\sin^{2k}\theta\cos 2n\theta\cos 2m\theta\,d\theta$ $(k=3)$

m/n	0	1	2	3	4	5	6	7	8	9	10
0	**5/8**	−15/32	3/16	−1/32	0						
1	−15/32	**13/32**	−1/4	3/32	−1/64	0					
2	3/16	−1/4	**5/16**	−15/64	3/32	−1/64	0				
3	−1/32	3/32	−15/64	**5/16**	−15/64	3/32	−1/64	0			
4	0	−1/64	3/32	−15/64	**5/16**	−15/64	3/32	−1/64	0		
5		0	−1/64	3/32	−15/64	**5/16**	−15/64	3/32	−1/64	0	
6			0	−1/64	3/32	−15/64	**5/16**	−15/64	3/32	−1/64	0

Manuscript receiced May 19, 1999, and revision received Nov. 3, 1999.